The Astrophysical Journal, 698:1207–1220, 2009 June 20 doi:10.1088/0004-637X/698/2/1207

X-RAY VARIABILITY OF ACTIVE GALACTIC NUCLEI IN THE SOFT AND HARD X-RAY BANDS

V. R. Chitnis[1], J. K. Pendharkar[2], D. Bose[3,5], V. K. Agrawal[3], A. R. Rao[3], and R. Misra[4]
[1] Department of High Energy Physics, Tata Institute of Fundamental Research, Mumbai 400005, India
[2] Indian Institute of Astrophysics, II Block, Koramangala, Bangalore 560 034, India, and Physical Research Laboratory, Ahmedabad 380009, India
[3] Department of Astronomy and Astrophysics, Tata Institute of Fundamental Research, Mumbai 400005, India
[4] Inter-University Center for Astronomy and Astrophysics, Post Bag 4, Ganeshkhind, Pune 411007, India
Received 2008 May 21; accepted 2009 April 6; published 2009 May 28

ABSTRACT

We investigate the X-ray variability characteristics of hard X-ray-selected active galactic nuclei (AGNs)—based on *Swift*/Burst Alert Telescope—in the soft X-ray band using the *Rossi X-ray Timing Explorer*/All-Sky Monitor (*RXTE*/ASM) data. The uncertainties involved in the individual dwell measurements of the ASM are critically examined, and a method is developed to combine a large number of dwells with appropriate error propagation to derive long-duration flux measurements (greater than 10 days). We also provide a general prescription to estimate the errors in variability derived from rms values from unequally spaced data. Though the derived variability for individual sources is not of very high significance, we find that, in general, the soft X-ray variability is higher than that in hard X-rays, and the variability strengths decrease with energy for the diverse classes of AGNs. We also examine the strength of variability as a function of the break timescale in the power density spectrum (derived from the estimated mass and bolometric luminosity of the sources) and find that the data are consistent with the idea of higher variability at timescales longer than the break timescale.

Key words: black hole physics – galaxies: active – galaxies: nuclei – galaxies: Seyfert – X-rays: galaxies

1. INTRODUCTION

Time variable X-ray emission is a probe to the inner regions of active galactic nuclei (AGNs) and is considered to be one of their defining characteristics. X-ray variability studies provide insight into the geometry and the physical conditions in the nuclear regions on account of the fact that this emission is thought to be emitted from regions close to the supermassive black hole. X-ray variability studies on timescales of months to years in AGNs have established the similarity of the physical processes across stellar mass to supermassive black holes (Uttley & McHardy 2004; McHardy et al. 2006). Since the characteristic timescale is proportional to the mass of the black hole, $M_{\rm BH}$, continuous monitoring for a long duration becomes necessary in the case of AGNs based on linear scaling with black hole mass from X-ray binary systems.

Early studies on X-ray variability using data from *EXOSAT* in the 0.1–10 keV range showed that on short timescales AGN variability appeared to be red noise dominated. In other words, it was unpredictable and aperiodic in nature (McHardy & Czerny 1987). Corresponding power spectral density (PSD; i.e., variability power as a function of temporal frequency) is best fitted by a power law of slopes -1 to -2 with no cutoff seen down to the lowest sampled frequencies. However, the shapes of their PSDs were shown to be similar to those of X-ray binaries (XRBs) in their soft state (McHardy 1988). Hence, analogous to the high-frequency breaks seen in the PSDs of XRBs and assuming that the break timescale varies linearly with $M_{\rm BH}$, a break to flatter PSD slope was expected over a period of days to weeks. Due to the uneven sampling of data, the results yielding the break frequency were uncertain. The *EXOSAT* data of ∼day-long AGN X-ray observations have revealed an inverse correlation between the amplitude of variability and X-ray luminosity (Barr & Mushotzky 1986). Results from the *ROSAT* All-Sky Survey (RASS) on the soft X-ray variability of the AGN showed the variability strength on timescales of days to be a function of steepness of the X-ray spectrum with sources with steeper spectra exhibiting stronger variability (Grupe et al. 2001). PSD studies were constrained due to large time gaps between subsequent observations in *ROSAT* data.

With the launch of the *RXTE* in 1995, a significant improvement was seen in the quality of data and a manifold increase in the monitoring timescale, from months to years, was possible. Because of its rapid slewing capability and flexible scheduling, an evenly sampled long-term monitoring of AGN X-ray variability was carried out for several sources. In contrast to the results from the then existing satellites, AGN light curves from *RXTE*/PCA in the 2–20 keV energy band showed that on longer timescales, of about a month, sources displayed less dispersion in variability amplitudes compared to those measured on timescales of one day (Markowitz & Edelson 2001). The PSDs also revealed a cutoff/ break at long timescales correlated with their black hole mass (Edelson & Nandra 1999; Uttley et al. 2002; Markowitz et al. 2003), but with a large scatter in the correlation (Done & Gierlinski 2005). McHardy et al. (2006) ascribed this scatter to a third variable, accretion rate, and found that the break timescale combined with the accretion rate can predict the mass of the black hole all the way from Galactic X-ray binaries to supermassive AGNs. They postulated that the variability originates within the accretion disk and the break timescale is associated with the inner edge of the disk, which makes an inward movement with increasing accretion rate for a given black hole mass.

Since such a scenario makes a definitive suggestion of the accretion disk geometry, a study of variability with energy should be able to pin down the radiation processes in the inner accretion disk quite reliably. Recently, variability studies of the AGN at energies above 15 keV have been carried out by Beckmann et al. (2007). The data of the first nine months of the *Swift*/Burst Alert Telescope (*Swift*/BAT) All-Sky Survey in the 14–195 keV range of the 44 brightest AGNs revealed a tendency of unabsorbed or type 1 Seyfert galaxies to be less

[5] Current address: Universidad Complutense, E-28040 Madrid, Spain.

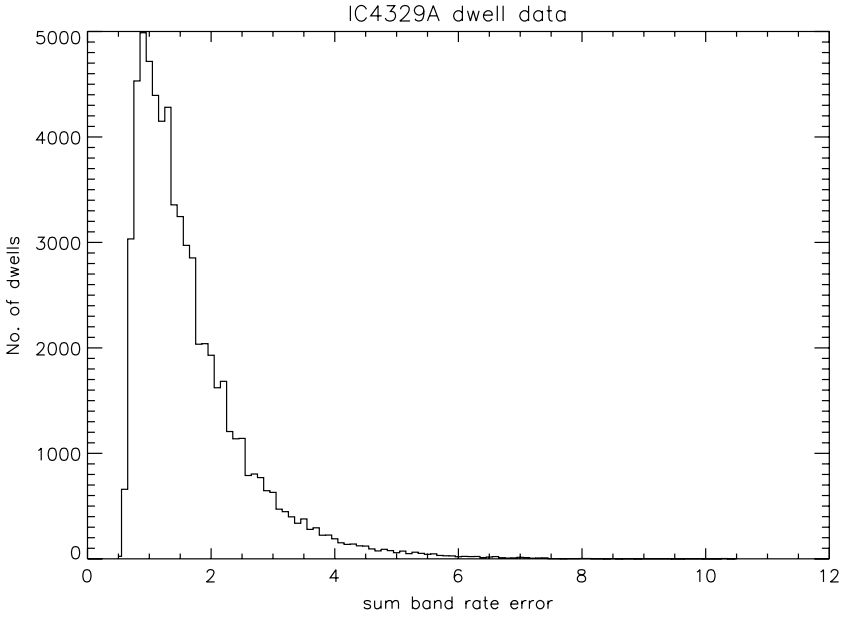

Figure 1. Distribution of errors on sum band rates from dwells for IC4329A.

variable than absorbed or type 2 objects. Also they found a more solid anticorrelation between variability and luminosity, which was previously detected in soft X-rays, UV, and optical bands.

The *RXTE*/ASM All-Sky Survey data give information on a large number of X-ray sources, including AGNs. The sensitivity (typically 10 mCrab for the one day average data) is not sufficient to make a detailed study of AGNs. By taking data at larger bin sizes, however, it should be possible to get meaningful information on the variability at longer timescales. In this paper, we have carried out a comparative study of the variability of AGNs in soft (< 12 keV) and hard (> 12 keV) X-ray bands using data from the *RXTE*/ASM All-Sky Survey and results obtained by Beckmann et al. from the *Swift*/BAT All-Sky Survey. Data selection is described in Section 2 followed by data analysis and results in Section 3 and discussion and conclusions in Section 4.

2. DATA SELECTION

The All-Sky Monitor (ASM; Levine et al. 1996) onboard *Rossi X-ray Timing Explorer* (*RXTE*; Swank 1999) consists of three Shadow Scanning Cameras (SSCs). Each SSC contains a position-sensitive proportional counter (PSPC) that views sky through a slit mask. The field of view (FOV) of each SSC is $6^\circ \times 90^\circ$, allowing the ASM to scan most of the sky every 1.5 hr. So apart from locating transient objects, it also provides photometric records of known sources in three energy bands corresponding to A (1.5–3 keV), B (3–5 keV), and C (5–12 keV) in addition to the total, or sum band, intensity in the 1.5–12 keV band. The MIT database (http://xte.mit.edu/ASM_lc.html), from where we have extracted ASM light curves, gives data dwell by dwell and one day average data points. In dwell by dwell, each raw data point represents the fitted source flux from one 90 s dwell, whereas in the case of the "one day average" each data point represents the one day average of the fitted source fluxes from a number (typically 5–10) of individual ASM dwells.

To have comprehensive information, we have selected all AGN candidates (147) from the ASM source list and carried out a systematic analysis. We found 31 AGNs from the sample used by Beckmann et al. (2007). We find measurable ASM flux for all the sources except two (NGC 1365 and GRS 1734-292). This sample of common sources consists of three blazars, one radio galaxy, eight Seyfert 1, four Seyfert 1.5, two Seyfert 1.8, one Seyfert 1.9, and 12 Seyfert 2. The BAT sources not in the ASM source list include one blazar, three Seyfert 1, one Seyfert 1.5, and eight Seyfert 2.

3. DATA ANALYSIS AND RESULTS

3.1. ASM Dwell Data Selection Criteria

We have downloaded all available ASM dwell data for 147 AGNs from the MIT database (http://xte.mit.edu/ASM_lc.html). This covers data from MJD 50087 to about 54466, i.e., 1996 January 5 to 2008 July 15. Dwell data are subjected to the usual selection cuts as prescribed by the ASM Web site and binned in 20 and 40 days bins. On closer inspection of the light curves of individual sources, several large spikes, some of them with an apparent periodicity of one year, were noticed. These abnormal data were found to have large intrinsic errors too. Since the estimation of count rates in the ASM is based on a profile-fitting method, the errors depend on the other sources in the FOV and on the orientation of the ASM FOV for a given observation. As a first cut, we examined the possibility that there could be enhanced unaccounted systematic errors for data points with large measured errors. It is found that the measured errors for each dwell data point are sharply peaked at 1 count s^{-1}. The distribution of errors for each dwell data point for one of the sources (IC4329A) is shown in Figure 1. Based on these considerations, we have introduced a selection criterion of an upper limit on sum count rate error of 3 counts s^{-1}, corresponding to three times the peak value of the distribution.

After selecting dwell count rates for sum, A, B, and C bands based on the above-mentioned cuts, they are binned into 20 and 40 days starting from MJD 50087. For each bin, the average rate and error are calculated for all the four bands as the weighted mean and estimated error of the mean. Data points with too few a number of individual dwell measurements (less than 20 data points for 20 day binning and less than 40 data points for 40 day binning) are also ignored, ensuring that there is at least one dwell

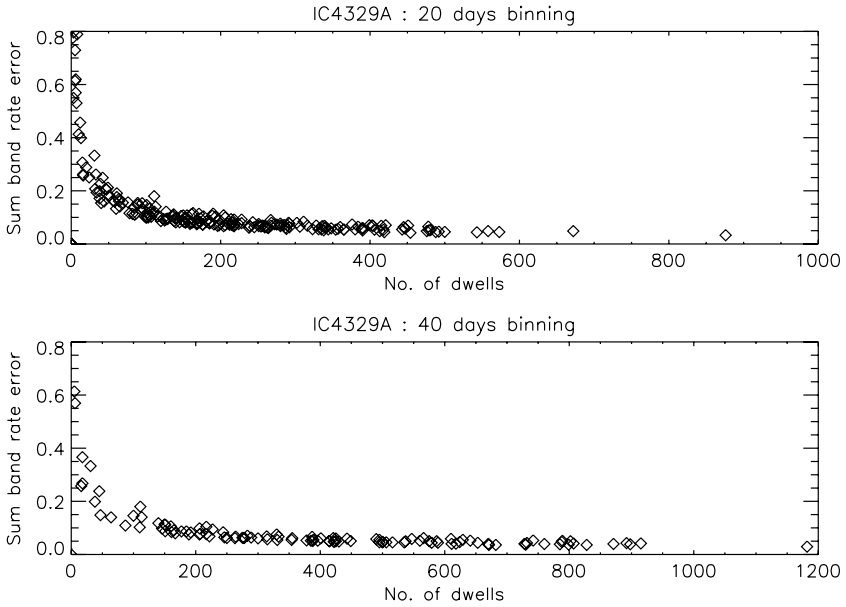

Figure 2. Sum rate error vs. no. of dwells for IC4329A with 20 days and 40 days binning.

per day on average. For example, for IC4329A, Figure 2 shows the sum band rate error after binning as a function of the number of dwells per bin for 20 and 40 days binning. In both cases, sum band error increases sharply for bins with a lower number of dwells. After introducing these criteria, the individual light curves are carefully examined, and no systematic abnormalities are found in them.

To summarize, the selection criteria for generating ASM light curves are as follows.

1. Reduced χ^2 of the fit < 1.5.
2. Number of sources in the FOV < 16.
3. Earth angle $> 75^\circ$.
4. Exposure time > 30 s.
5. Long-axis angle $-41.^\circ5 < \theta < 46^\circ$
6. Short-axis angle $-5^\circ < \phi < 5^\circ$.
7. Error on sum count rate < 3 counts s^{-1}.
8. Number of dwells for N day bin light curve is $> N$.

The first six selection criteria are the same as those used for generating one day average count rates from dwell data as described on the MIT database Web page.

3.2. ASM Light Curves

The ASM measurements have a systematic error of 3% added in quadrature to the statistical errors. This error is estimated using Crab light curves and could be underestimated in some cases (http://xte.mit.edu/ASM_lc.html). Grimm et al. (2002) have studied light curves of several sources with constant X-ray flux binned with different bin durations from one to 200 days and have estimated systematic error on large timescales in the range of 0.01–0.1 counts s^{-1}, depending on the source flux. According to Figure 2 of their paper, there seems to be a shift of about 10% between measured and estimated rms for sources with constant flux. We have investigated this in detail to get a better handle on the average systematic errors. For a few of the bright sources, we have generated the PSD using a method based on the autocorrelation function (Gilfanov & Arefiev 2005) and have assumed that the frequency-independent power has to be there due to the errors in each observations. Based on these PSD, the rms noise level seems to be underestimated by

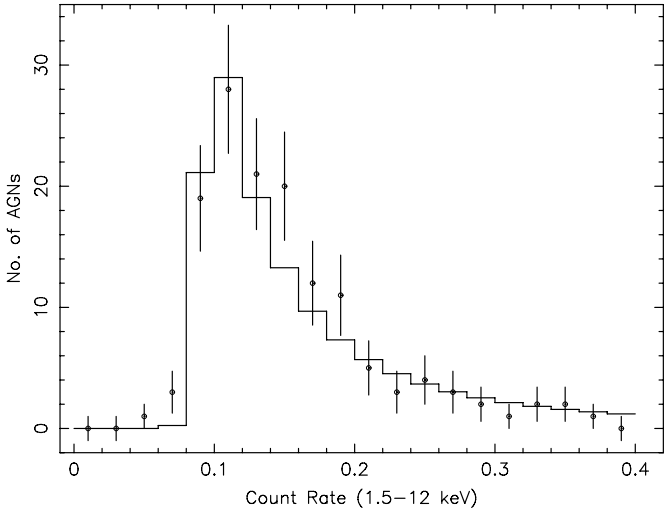

Figure 3. Histogram of ASM sum band count rates for 147 AGNs. Data are shown as points with error bars and the fit by a power law with the constant offset is shown as a histogram.

a factor of 1.13. A few steady sources were also investigated, and the frequency-independent systematic error is similar to this number. Though we cannot completely rule out some additional frequency-dependent systematic errors, we assume that for large bin sizes (greater than 10 days) most of the systematic errors are taken into account. This assumption is further strengthened by examining individual light curves as well as the distribution of the source fluxes (see below). After correcting the typical binned error of 0.005 counts s^{-1} with this factor, this systematic error translates into typical systematic error of 0.5 counts s^{-1} for dwell in the sum band and 0.3 counts s^{-1} for the A, B, and C bands.

According to the ASM data products page (http://xte.mit.edu/), there is a 1 mCrab positive bias in the light curve intensities. This bias is only evident when enough data are averaged so that the statistical uncertainties are driven to be very small. This generally requires binning or analyzing the light curves on timescales of many days or longer. In order to estimate this bias we have carried out the following exercise. We have

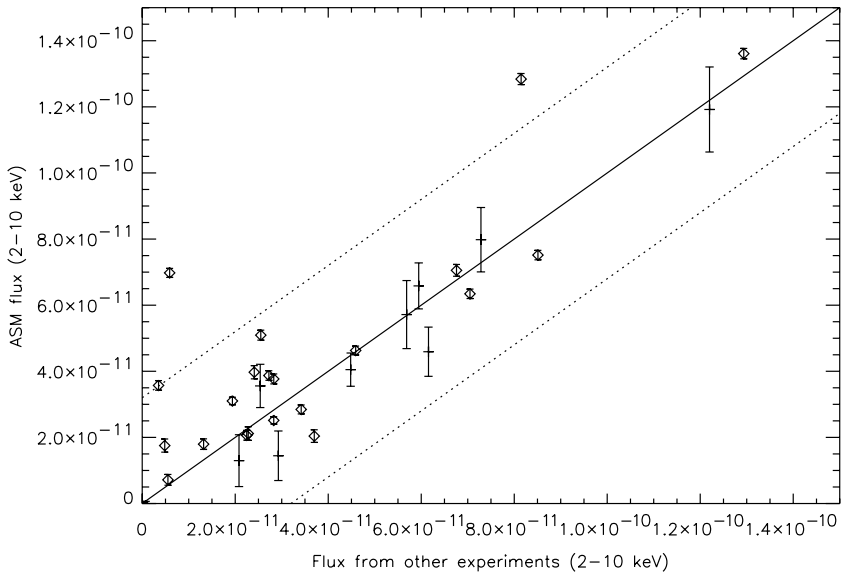

Figure 4. Absorbed ASM flux vs. observed flux (in units of erg cm^{-2} s^{-1}) from various experiments shown by diamonds. The ASM flux is derived from the average of the ASM count rate over a period of more than 10 years. The solid line corresponds to the case where the ASM flux is the same as the flux from other measurements. Dotted lines correspond to the ASM flux in the range of ±0.1 count s^{-1} around the solid line. Points indicated by plus signs (and large error bars) correspond to flux measurements from PCA onboard *RXTE* compared with simultaneous ASM measurements for IC4329A, NGC4151, NGC3783, MCG-6-30-15, 3C120, 3C390.3, NGC3227, NGC4051, and NGC3516.

generated a histogram of average sum band count rates for 147 AGNs (Figure 3). Unlike the usual number distribution given in an integral way, this is a differential plot and hence the number should vary with count rates as a power law with an index of −2.5 for an isotropic distribution. Hence, we have fitted this histogram with a function consisting of a power law with slope −2.5, and constant offset represented as the start point of the power law. Count rates were spread in the *x*-axis using a Gaussian distribution with $\sigma = 0.0056$ counts s^{-1} according to the above-mentioned error estimation. The fit for sum band data is shown in Figure 3. The number distribution is shown as data points with error bars (error taken as the square root of the number in each bin) and the fit is shown as a histogram. Offsets obtained with this method for various bands are as follows: sum band, 0.0895 counts s^{-1}; A band, 0.0274 counts s^{-1}; B band, 0.015 counts s^{-1}; C band, 0.0213 counts s^{-1}. These values are consistent with the 1 mCrab offset quoted on the ASM Web site.

As a further verification of these offsets and systematic error, we checked for consistency of flux estimates. We compared our results with the flux obtained from a uniform spectral analysis done on a large sample of AGNs (Winter et al. 2009) and found 22 common sources. Using the spectral parameters from Winter et al. (2009) and ASM sum band average count rates, we estimated the 2–10 keV absorbed flux for these sources using a Web calculator (WebPIMMS tool at http://heasarc.gsfc.nasa.gov/Tools). Figure 4 shows the plot of 10 year averaged absorbed ASM flux versus observed flux from other experiments, both in the energy range of 2–10 keV. It should be noted that these observations are not simultaneous. Hence source variability can cause nonidentical fluxes between the ASM and the other experiments. Points are marked by diamonds. The solid line corresponds to the case where the ASM flux is equal to flux measurements from other experiments. The dotted lines correspond to the ASM flux equivalent to ±0.1 counts s^{-1} around the solid line. Most of the sources barring a few like IC4329A and NGC 4388 are close to the fitted line, within ±0.1 ASM counts s^{-1}. As a further check, we compared the long duration *RXTE* PCA measurements from the uniform analysis done by Markowitz & Edelson (2004). We found these measurements for nine sources: IC4329A, NGC4151, NGC3783, MCG-6-30-15, 3C120, 3C390.3, NGC3227, NGC4051, and NGC3516 (Markowitz & Edelson 2004). We estimated the ASM flux by extracting 40 days binned sum band rates almost simultaneous with the PCA measurements. These points are indicated by the plus signs with the error bars in the plot. Hence overall there is a good agreement between flux estimates from the ASM and other observations. This agreement also justifies our estimates of count rate offsets and systematic errors. We note here that further refinement in the flux comparison is difficult to achieve because of the fact that at shorter timescales (where pointed observations are available) the ASM error bars are too large and at longer timescales (when the ASM error bars are driven to a small value) pointed observations are simply not available.

Applying the above-mentioned cuts and corrections, light curves in all four bands were generated for all ASM-detected AGNs. Average sum band count rates of all these AGNs in four bands with 20 days binning for 30 sources common to the ASM and BAT databases are given in Table 1. There was one more common source, GRS 1734-292, which was rejected after applying the above-mentioned cuts. That is, there was no single stretch of 20 days with at least 20 dwells satisfying all the cuts (possibly because of its proximity to the Galactic center). Count rates given in Table 1 are weighted means of binned counts rates and the estimated error on the mean. Out of these, 15 sources have average sum band count rates above 0.2 counts s^{-1}. Some of these sources (11) are common sources in the BAT and ASM databases and are included in Table 1. The remaining sources are 1ES1959+650, IGR J18027-1455, MCG 6-30-15, and Mrk 501. Light curves for these 15 sources with 20 days binning are given in Figures 5–7.

The literature survey for *RXTE*/PCA light curves of AGNs (in this study) accumulated over long periods has allowed us to compare them with those of long looks of the ASM. We could obtain PCA light curves for Mrk 501 and Mrk 421 taken over

Table 1
Variability Strength and Break Timescale (T_B) for the ASM Sample

Source Name	ASM Rate (1.2–15 keV) (counts s^{-1})	ASM Luminosity $\log(L_{ASM})$ (erg s^{-1})	ASM Variability Strength[1] S_v 1.5–12 keV	1.5–3 keV	3–12 keV	BAT[1] Variability Strength S_v	BH Mass ($\log M_{BH}$) ($M_\odot$)	$\log(L_{bol})$ (ergs s^{-1})	$\log(T_B)$ (days)	Type
3C273	0.280 ± 0.004	45.68	34.7 ± 3.4	64.7 ± 7.9	33.6 ± 4.4	15 ± 5	7.22	47.35	−3.04	Blazar
3C454.3	0.078 ± 0.006	46.59	...	...	...	42 ± 12	9.17	47.27	1.13	Blazar
Mrk421	0.894 ± 0.005	44.57	83.7 ± 4.2	79.4 ± 4.1	88.4 ± 4.5	142 ± 38	8.29	∼45.00	1.51	Blazar
IGR J21247 + 5058	0.126 ± 0.004	43.54	42.3 ± 5.0	...	51.4 ± 5.0	11 ± 6	...	...	...	Radio galaxy
3C120	0.173 ± 0.005	44.11	42.7 ± 6.3	64.1 ± 7.9	38.9 ± 10.4	$\leqslant 10$	7.42	45.34	−0.65	Sy1
3C390.3	0.109 ± 0.004	44.37	29.7 ± 5.3	49.6 ± 9.4	30.5 ± 7.5	$\leqslant 6$	8.55	44.88	2.17	Sy1
EXO0556-386	0.069 ± 0.005	43.74	...	76.8 ± 14.1	...	$\leqslant 9$	...	...	...	Sy1
IC4329A	0.459 ± 0.006	43.91	22.7 ± 2.5	48.0 ± 4.5	18.1 ± 3.5	$\leqslant 3$	6.77	44.78	−1.47	Sy1
MR2251-178	0.134 ± 0.005	44.57	51.2 ± 8.4	96.7 ± 22.5	42.3 ± 13.5	$\leqslant 7$	...	...	...	Sy1
NGC3783	0.222 ± 0.005	43.16	28.5 ± 4.9	67.3 ± 12.8	24.1 ± 7.4	$\leqslant 4$	6.94	44.41	−0.75	Sy1
NGC4593	0.105 ± 0.005	42.76	79.7 ± 11.2	...	71.3 ± 21.8	$\leqslant 7$	6.91	44.09	−0.50	Sy1
NGC3227	0.125 ± 0.005	42.10	56.2 ± 7.1	123.2 ± 17.6	49.3 ± 11.4	$\leqslant 14$	7.64	43.86	1.26	Sy1.5
NGC3516	0.091 ± 0.004	42.68	76.6 ± 7.0	...	72.0 ± 9.6	$\leqslant 7$	7.36	44.29	0.25	Sy1.5
NGC4051	0.064 ± 0.005	41.31	...	...	...	$\leqslant 9$	6.13	43.56	−1.62	Sy1.5
NGC4151	0.434 ± 0.005	42.51	53.9 ± 3.2	136.3 ± 12.5	53.3 ± 3.2	27 ± 7	7.13	43.73	0.32	Sy1.5
NGC1365	< 0.005	...	...	...	...	$\leqslant 17$	...	...	...	Sy1.8
MCG-05-23-016	0.263 ± 0.005	43.11	32.8 ± 3.6	...	32.2 ± 4.6	6 ± 4	7.60	44.21	2.85	Sy1.9
NGC5506	0.237 ± 0.006	42.79	42.9 ± 4.6	...	47.7 ± 5.2	$\leqslant 3$	8.00	44.53	1.36	Sy1.9
CenA	0.674 ± 0.006	42.19	32.7 ± 1.9	73.4 ± 7.9	35.9 ± 2.0	10 ± 2	8.38	43.0	3.66	Sy2
CygnA	0.331 ± 0.005	44.85	25.8 ± 2.4	36.0 ± 4.1	27.7 ± 3.0	$\leqslant 7$	9.40	46.0	2.86	Sy2
ESO103-G35	0.120 ± 0.006	43.16	69.5 ± 9.0	76.8 ± 14.1	74.3 ± 10.1	$\leqslant 8$	...	...	...	Sy2
Mrk348	0.054 ± 0.006	42.91	...	...	...	12 ± 10	7.21	44.27	−0.04	Sy2
NGC1275	2.541 ± 0.005	44.73	4.62 ± 0.41	5.6 ± 0.8	4.7 ± 0.5	$\leqslant 14$	8.51	45.04	1.93	Sy2
NGC2110	0.168 ± 0.005	42.84	41.7 ± 5.3	69.7 ± 13.9	28.4 ± 7.6	25 ± 7	8.30	44.10	2.41	Sy2
NGC2992	0.122 ± 0.005	42.69	101.7 ± 8.1	128.1 ± 14.4	118.6 ± 11.1	45 ± 19	7.72	43.92	1.37	Sy2
NGC3081	0.022 ± 0.005	41.98	...	...	...	23 ± 11	...	...	...	Sy2
NGC4388	0.204 ± 0.004	42.99	17.6 ± 7.8	36.0 ± 10.6	32.6 ± 15.3	11 ± 4	...	...	...	Sy2
NGC4507	0.062 ± 0.006	42.77	...	...	...	$\leqslant 8$	...	...	...	Sy2
NGC7172	0.063 ± 0.006	42.52	...	...	...	12 ± 9	...	...	...	Sy2
NGC7582	0.056 ± 0.005	42.02	...	...	...	23 ± 21	...	...	...	Sy2
Mrk3	...	...	...	...	...	± 7	8.65	44.54	2.72	Sy2
1ES1959 + 650	0.243 ± 0.003	44.26	55.8 ± 3.0	56.9 ± 3.4	60.4 ± 3.6	...				Blazar
IGRJ18027-1455	0.254 ± 0.010	43.64	42.3 ± 5.0	77.1 ± 14.7	70.4 ± 12.1	...				Sy1
MCG-6-30-15	0.208 ± 0.006	44.65	34.3 ± 5.7	69.1 ± 7.8	40.2 ± 8.7	...	6.65	43.56	−0.52	Sy1
Mrk 501	0.368 ± 0.004	43.27	76.7 ± 3.9	62.1 ± 3.6	90.4 ± 4.7	...	9.21			Blazar
Crab	75.355 ± 0.010	...	0.48 ± 0.03	1.25 ± 0.07	0.37 ± 0.03	1.27	...	....	...	Pulsar

Note.
[1] ASM variability strengths are computed for data spanning a duration of 12.5 years, whereas BAT variability strengths correspond to data collected over nine months. Bin size is 20 days for both the cases.

a period of eight and nine years, respectively, overlapping with the period for ASM light curves. The data set for Mrk 421 covers a period 1996–2005 (Figure 1 of Emmanoulopoulos & Wagner 2007) and 1997–2004 for Mrk 501 (Gliozzi et al. 2006). Peaks at similar MJDs are identified on inspecting the ASM and PCA light curves for Mrk 421. The peaks were found near MJDs 51000, 51700, 51900, 52600, and 53100. Similarly, peaks for Mrk 501 were found near the time 1997 (MJD 50600).

3.3. Variability Strength

We have calculated the strength of variability for all these sources in bin sizes of 20 and 40 days. The strength of variability and the errors on them are calculated as follows.

A light curve from a source consists of N flux measurements x_i with measurement errors of σ_i. In addition to these variations, the object has intrinsic variability or additional source variance σ_Q. It is necessary to disentangle these two variances. One of the approaches to estimate the intrinsic variability is to use an *excess variance* σ_{XS} as an estimator (Nandra et al. 1997; Vaughan et al. 2003). It is given by

$$\sigma_{XS}^2 = S^2 - \overline{\sigma_i^2}, \quad (1)$$

where the sample variance S^2 is given by

$$S^2 = \frac{1}{N-1}\sum (x_i - \overline{x})^2, \quad (2)$$

where $\overline{x}$ is the mean rate, and $\overline{\sigma_i^2}$ is the average variance of the measurements.

For light curves with varying measurement uncertainties ($\sigma_i \neq$ constant), it is necessary to use a numerical approach to obtain the best estimate for the parameter of interest (σ_Q here; Almaini et al. 2000). The most widely used method for this purpose is the principle of maximum likelihood. The probability density of obtaining data values x_i is given as a product of Gaussian functions. Using Bayes' theorem a probability

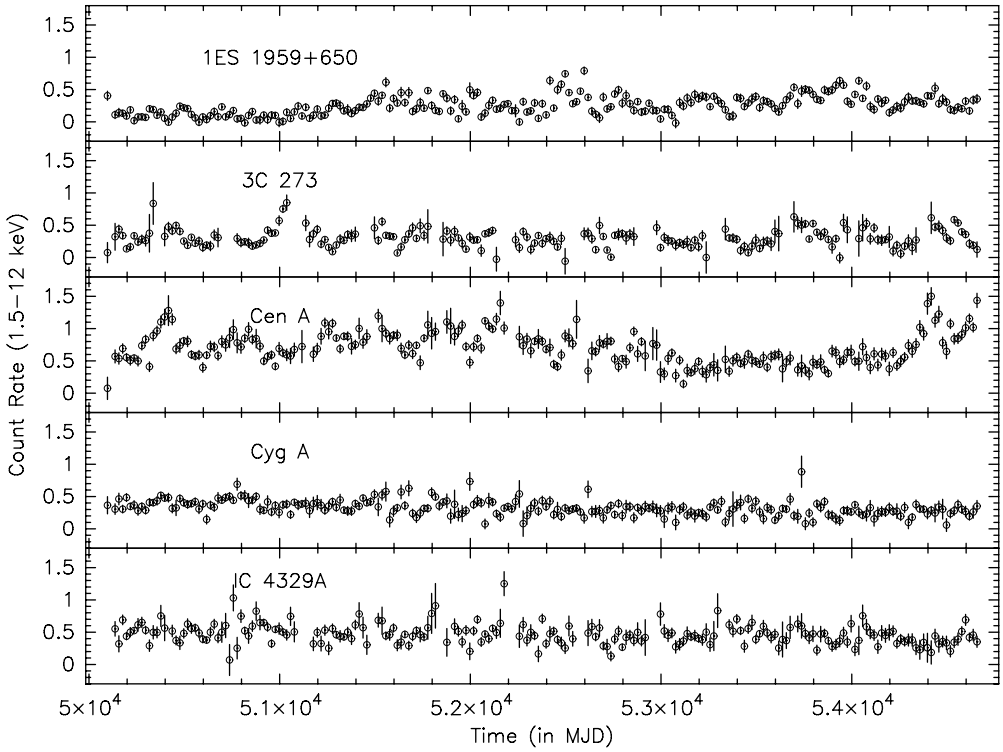

Figure 5. ASM sum band light curves (1.5–20 keV) for 1ES 1959 + 650, 3C 273, Cen A, Cyg A, and IC 4329A with 20 days binning.

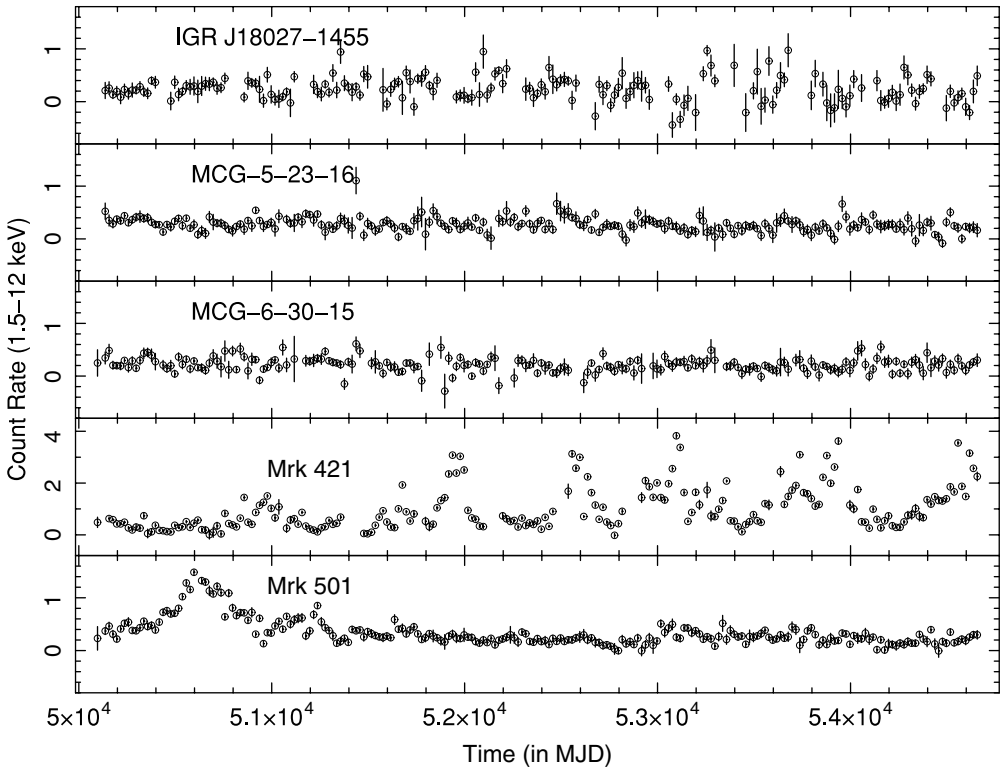

Figure 6. ASM sum band light curves (1.5–20 keV) for IGR J18027-1455, MCG-5-23-16, MCG-6-30-15, Mrk 412, and Mrk 501 with 20 days binning.

distribution for σ_Q is obtained. This is a likelihood function for σ_Q, and it can be calculated assuming Bayesian prior distributions for σ_Q and x_i. By differentiating, the maximum likelihood estimate can be obtained for σ_Q (see Beckmann et al. 2007 for equations). In the case of identical measurement errors (σ_i = constant), this expression reduces to excess variance for uniform prior. This corresponds to $\sigma_Q = \sigma_{\rm XS}$. In the present analysis of ASM data, since σ_i is almost constant we have used this simplified approach. This assumption about the approximate constancy of the σ_i is established using IC4329A data. Figure 8 shows the distribution of the sum rate error after 20 days and 40 days binning, after applying a cut on the number of dwells

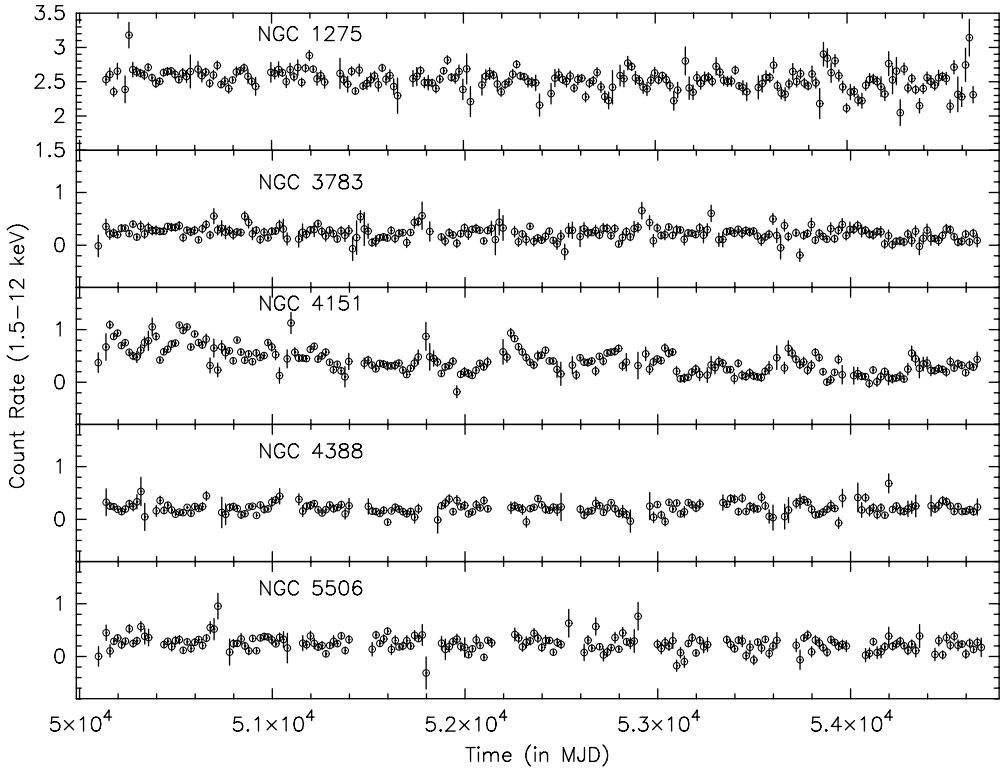

Figure 7. ASM sum band light curves (1.5–20 keV) for NGC 1275, NGC 3783, NGC 4151, NGC 4388, and NGC 5506 with 20 days binning.

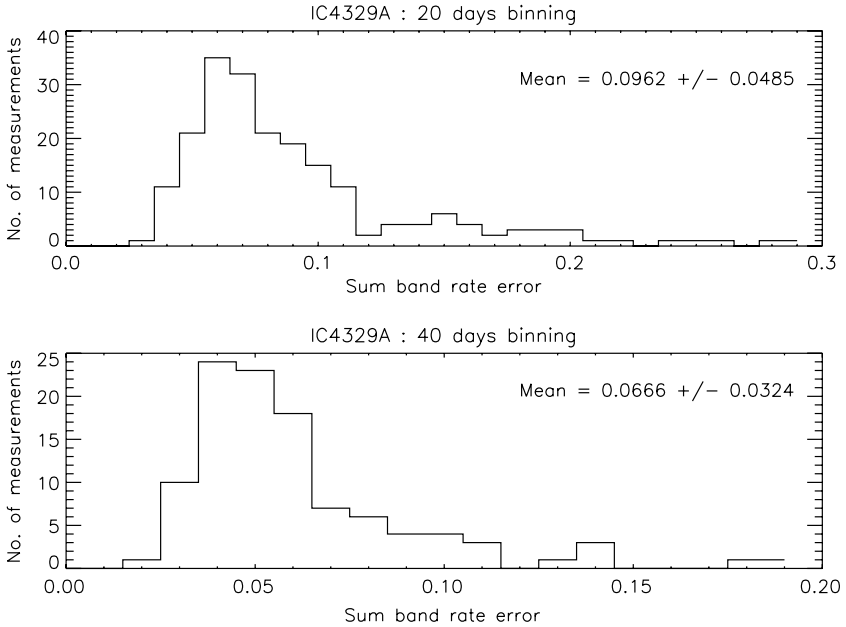

Figure 8. Distribution of sum rate errors with 20 days and 40 days binning for IC4329A after a cut on number of dwells.

per bin. The mean value of the binned sum rate error and rms is given in the figure. These distributions are sufficiently narrow to validate the assumption that the σ_i are constant.

Variability is given in terms of the normalized excess variance, i.e., $\sigma^2_{\rm NXS} = \sigma^2_{\rm XS}/\overline{x}^2$, or the fractional rms variability amplitude ($F_{\rm var}$) given by

$$F_{\rm var} = \sqrt{\frac{S^2 - \overline{\sigma_i^2}}{\overline{x}^2}}. \quad (3)$$

The error on the variability or normalized excess variance consists of two parts: (1) arising from measurement error, and (2) arising from intrinsic fluctuations, depending on the index of the power spectrum. So $\mathrm{err}(\sigma^2_{\rm NXS})$ is given by

$$\left[\mathrm{err}\left(\sigma^2_{\rm NXS}\right)\right]^2_T = \left[\mathrm{err}\left(\sigma^2_{\rm NXS}\right)\right]^2_M + \left[\mathrm{err}\left(\sigma^2_{\rm NXS}\right)\right]^2_I, \quad (4)$$

where the subscript T stands for the total error, M for the measurement error, and I for the intrinsic error. According to

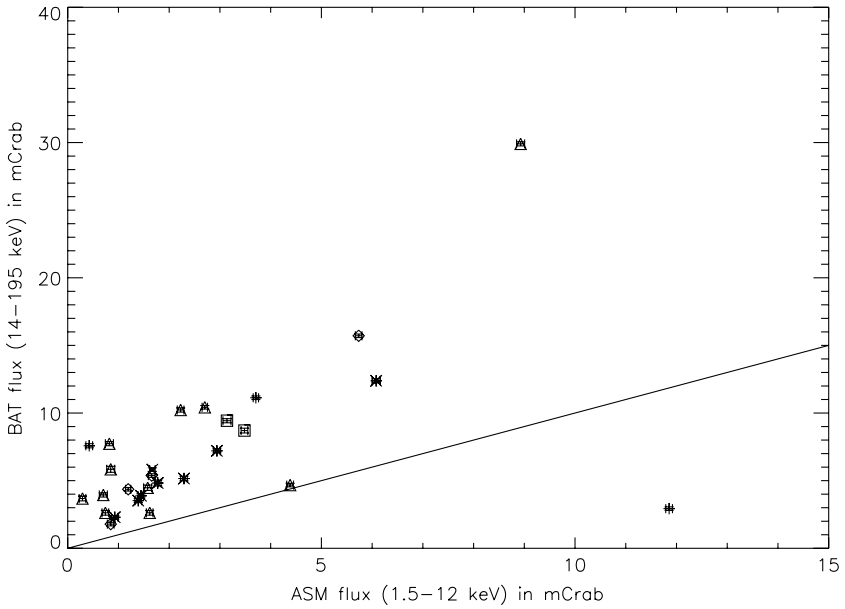

Figure 9. BAT flux (14–195 keV) vs. ASM flux (1.5–12 keV) for a sample of 30 AGNs common in the BAT and ASM databases. Blazars are indicated by the + sign, Seyfert 1 by the asterisk, Seyfert 1.5 by the diamond, Seyfert 1.8 and 1.9 by the square, Seyfert 2 by the triangle, and radio galaxy by the cross. The solid line indicates slope 1.

Equation (11) from Vaughan et al. (2003),

$$\left[\mathrm{err}\left(\sigma_{\mathrm{NXS}}^2\right)\right]_M^2 = \frac{2}{N}\frac{\left(\overline{\sigma_i^2}\right)^2}{\overline{x}^4} + \frac{4\overline{\sigma_i^2}}{N}\frac{F_{\mathrm{var}}^2}{\overline{x}^2}. \quad (5)$$

Also, approximating intrinsic fluctuations with white noise (it should be noted that the light curves are red noise and white noise is assumed here for simplicity) and following Vaughan et al. (2003),

$$\left[\mathrm{err}\left(\sigma_{\mathrm{NXS}}^2\right)\right]_I = \sqrt{\frac{2}{N}}\sigma_{\mathrm{NXS}}^2 = \sqrt{\frac{2}{N}}F_{\mathrm{var}}^2. \quad (6)$$

Combining Equations (5) and (6), we get

$$\left[\mathrm{err}\left(\sigma_{\mathrm{NXS}}^2\right)\right]_T^2 = \frac{2}{N}\left(\frac{\overline{\sigma_i^2}}{\overline{x}^2} + F_{\mathrm{var}}^2\right)^2. \quad (7)$$

Substituting for F_{var} from Equation (3), we get

$$\left[\mathrm{err}\left(\sigma_{\mathrm{NXS}}^2\right)\right]_T^2 = \frac{2}{N}\left(\frac{S^2}{\overline{x}^2}\right)^2. \quad (8)$$

Hence

$$\left[\mathrm{err}\left(\sigma_{\mathrm{NXS}}^2\right)\right]_T = \sqrt{\frac{2}{N}}\frac{S^2}{\overline{x}^2}. \quad (9)$$

Following Equation (B2) of Vaughan et al. (2003),

$$\mathrm{err}(F_{\mathrm{var}})_T = \frac{1}{2F_{\mathrm{var}}}\mathrm{err}\left(\sigma_{\mathrm{NXS}}^2\right). \quad (10)$$

This is valid when $\mathrm{err}(\sigma_{\mathrm{NXS}}^2)$ is small and we get the following expression:

$$\mathrm{err}(F_{\mathrm{var}})_T = \frac{1}{\sqrt{2N}}\frac{S^2}{\overline{x}^2 F_{\mathrm{var}}}. \quad (11)$$

When $\mathrm{err}(\sigma_{\mathrm{NXS}}^2)$ is large, the error estimate will only be approximate. The strength of variability is calculated from the expression $S_{\mathrm{V}} = 100\% \times \sigma_Q/\overline{x}$, i.e., $S_{\mathrm{V}} = 100\% \times F_{\mathrm{var}}$.

We have applied this method to the downloaded light curves with different binning (20 and 40 days), and estimated σ_Q, i.e., intrinsic variability, as well as the variability strength S_{V} for all ASM-detected AGNs. This exercise is carried out for the sum band light curve over 1.5–12 keV, the A band (i.e., 1.5–3 keV), as well as the (B + C) band (i.e., 3–12 keV). Variability strengths for 20 and 40 days binning were found to be similar. Results for 20 days binning for sum band data are given in Table 1 for 30 AGNs which are common between the ASM and BAT databases. We have also listed ASM variability strengths for four AGNs with ASM count rates above 0.2 counts s^{-1}, but not detected by the BAT. Also included in the table is the BAT variability strength for Mrk 3, which is not detected by the ASM. In view of unknown systematics in the ASM data, we have quoted ASM variability strengths in various bands only for sources with count rates above 0.0895 counts s^{-1} for the sum band and 0.0274 counts s^{-1} for the A band. BAT variability strengths given in this table are from Beckmann et al. (2007). We have quoted their results as upper limits for the sources where their estimates of variability strength are negative or smaller than the error on the estimate.

Since X-ray spectral parameters (like the power-law index) are not available for all these sources, we have calculated the X-ray luminosities by converting the ASM sum band rates (R counts s^{-1}) to energy flux using

$$F[\mathrm{erg\ cm^{-2}\ s^{-1}}] = 3.2 \times 10^{-10} \times R[\mathrm{counts\ s^{-1}}]. \quad (12)$$

This assumes a Crab-like spectrum, as prescribed by Grimm et al. (2002). It should be noted that this assumption is not strictly valid for absorbed sources. For these sources, the photon index, over the A band in particular, could be much flatter than that of Crab. For the sources where spectral parameters are available, we get an average conversion factor very close to this value ($3.0 \times 10^{-10} \times R$ [counts s^{-1}]).

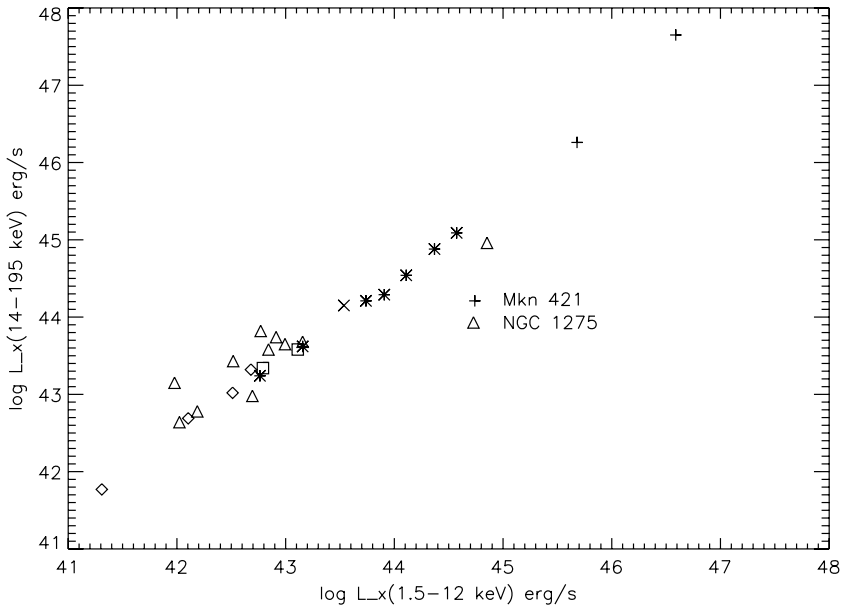

Figure 10. Hard X-ray luminosity of the AGN from the BAT vs. soft X-ray luminosity from the ASM for 30 common AGNs. Blazars are indicated by the + sign, Seyfert 1 by the asterisk, Seyfert 1.5 by the diamond, Seyfert 1.8 and 1.9 by the square, Seyfert 2 by the triangle, and radio galaxy by the cross.

To compare the flux in Crab units, we have used a conversion factor of 75.5 counts s^{-1} (ASM sum band) and 453.8 counts s^{-1} for BAT rates as given by Beckmann et al. (2007). This allows easy comparison of fluxes in two different energy bands. Figure 9 shows the variation of BAT flux versus ASM total flux in the energy range of 1.5–12 keV. Blazars are indicated by the plus signs, Seyfert 1 by the asterisks, Seyfert 1.5 by the diamonds, Seyfert 1.8 and 1.9 by the squares, Seyfert 2 by the triangles, and radio galaxy by a cross. Error bars are indicated for both the BAT and ASM fluxes. Typically, these error bars are smaller than the symbol size. One blazar, Mrk 421, and one Seyfert 2 galaxy, NGC1275 (not shown in the figure), seem to have much higher flux in the ASM compared to the other AGN with similar flux values in the BAT energy band. Mrk 421 is highly variable source as can be seen from the ASM light curve. BAT data correspond to only nine months out of 12.5 years of data accumulated by the ASM. (Mrk 421 was in a somewhat low state during the BAT observations.) In the case of NGC 1275, the ASM flux is about 33.7 mCrab, whereas the BAT flux is 4.5 mCrab. The FOV of NGC 1275 contains the Perseus cluster, and X-ray emission from this cluster could be responsible for a higher count rate and dilution of observed X-ray variability as indicated by much lower variability strength for this source (Sanders & Fabian 2007). The solid line in the figure indicates both fluxes being linearly related (as will be the case if the spectral slope of AGNs is crab like—a photon index of 2). The BAT flux seems to be increasing rapidly relative to the ASM flux. The lack of a strong correlation between the ASM and BAT fluxes could be due to the mixing of different types of objects: sources with very soft spectra which could be preferentially observed by the *ROSAT* satellite do not show flux correlation between the soft and hard bands (Tueller et al. 2008), whereas heavily obscured sources are obviously not expected to show correlation (because the very soft flux in these sources may not be originating from the central engine of the AGN).

Figure 10 shows luminosity of AGNs from BAT data as given by Beckmann et al. (2007) versus ASM luminosity. On a logarithmic scale, BAT luminosity seems to be increasing linearly with ASM luminosity. There are two AGNs which are slightly away from the trend shown by the other AGNs. These are the blazar (Mrk 421) and Seyfert 2 (NGC 1275) as in the case of Figure 9.

Table 2
Average Variability Strengths in Different Energy Ranges

Energy Range	All Sources	Blazars	Sy 1–1.5	Sy 1.8–2
ASM (1.5–12 keV)	41.1 ± 0.8	57.3 ± 1.7	38.4 ± 1.4	34.1 ± 1.2
ASM (1.5–3 keV)	61.4 ± 1.5	64.7 ± 2.0	64.0 ± 2.9	51.5 ± 3.0
ASM (3–12 keV)	44.3 ± 1.0	64.2 ± 1.9	39.1 ± 1.9	36.4 ± 1.4
BAT (14–195 keV)	12.6 ± 1.3	17.2 ± 3.6	19.2 ± 5.3	11.4 ± 1.5

Figure 11 shows the plot of ASM and BAT variability strength in different energy ranges. The top panel shows ASM variability strength in the 1.2–3 keV band, the second panel shows ASM variability strength in the 3–12 keV band, and the third panel shows BAT variability strength in the 14–195 keV band as a function of ASM variability strength in the 1.5–12 keV range. The bottom panel also shows BAT variability strength in the 14–195 keV band as a function of ASM variability strength in the 1.5–12 keV range for near-simultaneous data. Here we have selected ASM data corresponding to the first nine months of BAT operation. Error bars on ASM variability strength in this panel are large and for some of the sources only upper limits on variability strength could be estimated for the ASM data. For the sake of clarity, we have restricted the *x*-axis range to 120 for all the panels. The bottom-most panel has three points with ASM variability strength exceeding this value. The solid line in each panel corresponds to slope 1. It can be seen that variability strength decreases with increase in the energy range from 1.2–3 keV to 14–195 keV. Variability strength in the 3–12 keV band seems to be well correlated and almost similar to the one in the 1.5–12 keV band, indicating that in these two energy bands most of the flux is in the large overlapping energy range. To investigate this further, we have grouped the sources into three groups: (1) 3 blazars and one radio galaxy, (2) 7 Seyfert 1 and 4 Seyfert 1.5 galaxies, and (3) 1 Seyfert 1.8, 2 Seyfert 1.9, and 11 Seyfert 2 galaxies. Figure 12 shows distributions of variability strengths in the 1.5–12 keV,

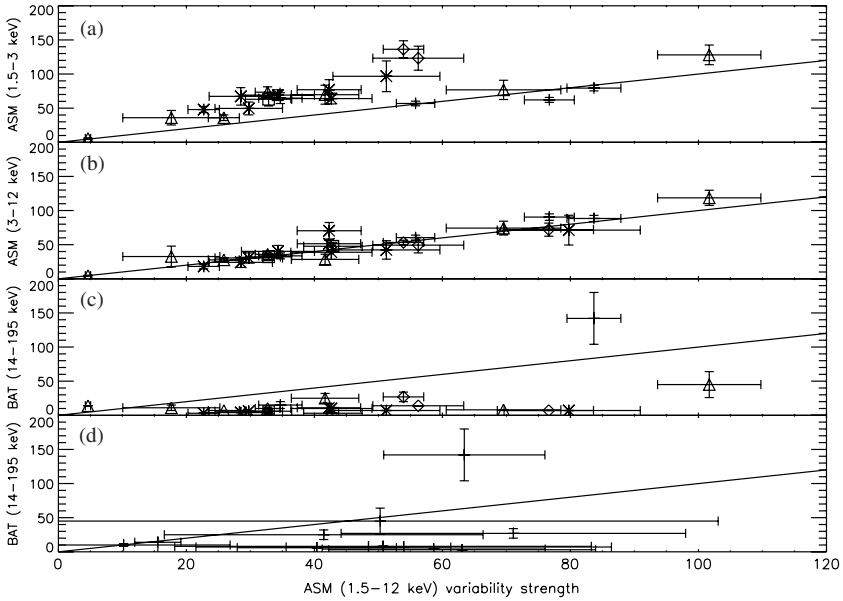

Figure 11. (a) ASM variability strength in the 1.5–3 keV band, (b) ASM variability strength in the 3–12 keV band (c) BAT variability strength in the 14–195 keV band as a function of ASM variability strength in the 1.5–12 keV band and (d) BAT variability strength in the 14–195 keV band as a function of ASM variability strength in the 1.5–12 keV band for simultaneous data. Variability strength decreases at higher energies.

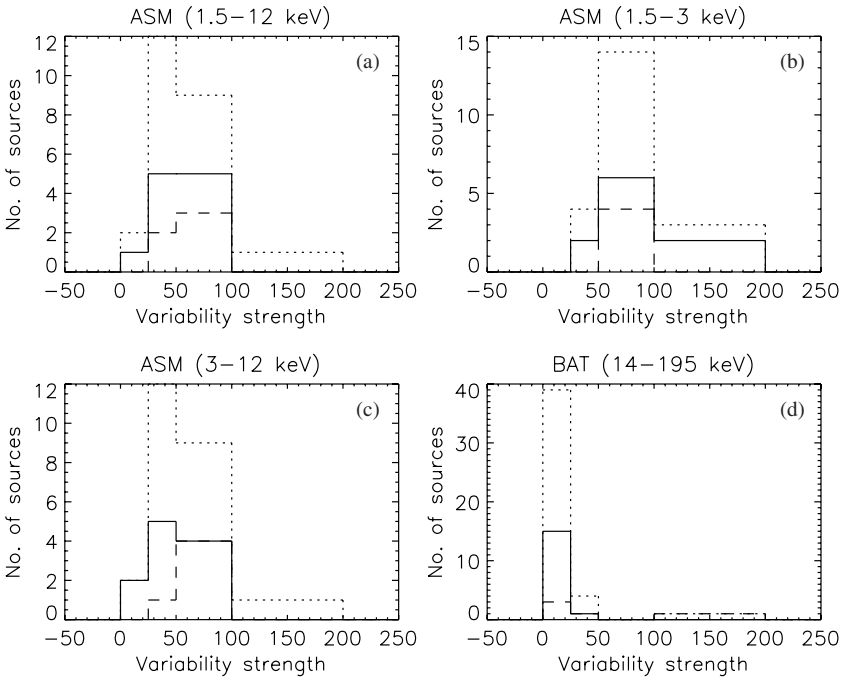

Figure 12. Distribution of variability strengths of the AGN in the (a) 1.5–12 keV, (b) 1.5–3 keV, (c) 3–12 keV, and (d) 14–195 keV bands as obtained from the ASM and BAT data. In each panel, the dotted line represents the distribution including all objects, the dashed line corresponds to blazars and radio galaxy, and the solid line represents the variability strength distribution for Seyfert 1 and 1.5 galaxies.

1.5–3 keV, 3–12 keV, and 14–195 keV bands. The dotted line corresponds to the histogram generated including all sources, the dashed line corresponds to blazars (i.e., group 1), and the solid line corresponds to Seyfert 1 and 1.5 (i.e., group 2). This figure includes BAT variability strengths given as upper limits in Table 1. Average values of variability strengths for different groups and for different energy ranges are listed in Table 2. Values given here are the weighted mean and estimated error on the mean. BAT variability strengths given as upper limits in Table 1 are not included here. NGC 1275 is excluded here for the ASM in these calculations since the variability strength for this object quoted here could be grossly underestimated due to contamination caused by the Perseus cluster in the FOV of the ASM. This table clearly shows the trend of decrease in variability strength with increase in energy for all types of AGNs.

The higher variability strength in the 1.5–3 keV band compared to that in the 3–12 keV band for Seyfert 1s is consistent with previous findings (see Arévalo et al. 2008 and references therein). They have found that the variability as a function of energy peaks around 2 keV on timescales of one to a few days. Our result extends this property to longer timescales.

We have compared our results with the variability strength in the 2–12 keV range from *RXTE*/PCA as presented by

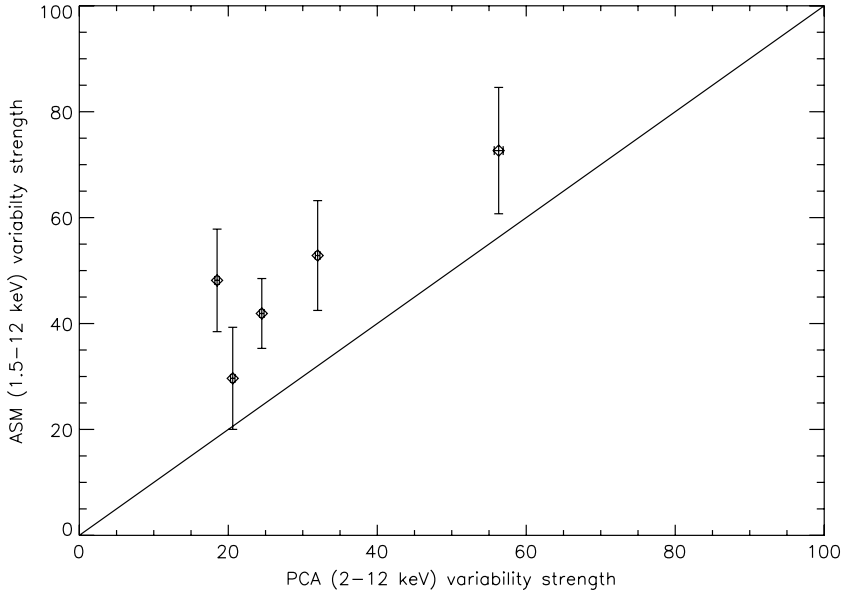

Figure 13. ASM variability strength (1.5–12 keV) vs. *RXTE*/PCA variability strength (2–12 keV) for Seyfert 1 and Seyfert 1.5 galaxies.

Table 3
Spectral Fits

Source Name	Observation Duration (s)	N_H (10^{22} cm^{-2})	Power-law Index	2–10 keV Flux (erg cm^{-2} s^{-1})
3C 273	2962.6	0.0316	1.79 ± 0.030	5.87×10^{-11}
3C 454.3	13670.0	0.0631	1.32 ± 0.02	5.43×10^{-11}
Mrk 421	6958.0	0.001	2.38 ± 0.01	8.34×10^{-11}
Cen A	7699.5	12.59	1.64 ± 0.06	1.99×10^{-10}

Markowitz & Edelson (2004). They have given variability strength for several Seyfert 1 and 1.5 galaxies on different timescales. There are five sources common between their sample with timescale of 1296 days (Table 3 in their paper) and the present sample. These are 3C120, NGC 3783, NGC 3516, MCG-6-30-15, and NGC 3227. For these sources, we have computed average variability strength in the energy range of 1.5–12 keV with 40 days binning covering roughly the same MJD range as Markowitz & Edelson (2004). The bin size of 40 days used here is close to the 34.4 days bin size used by them. Figure 13 shows the comparison of ASM variability strengths in the 1.5–12 keV range with PCA variability in the 2–12 keV range. ASM variability seems to be higher than the PCA variability.

3.4. Variability Strength versus Break Timescale

AGN variability is often expressed in terms of fluctuations in PSD, i.e., variability power $P(\nu)$ as a function of frequency, ν. On longer timescales, the PSDs of AGNs are fitted by a power law of slope -1 which breaks to a steeper slope (> 2) at timescales shorter than the "break" timescale, T_B (Markowitz et al. 2003). Break timescale is expected to depend on the black hole mass. Considering similarities between PSDs of X-ray binaries and AGNs, break timescales for AGNs are expected to be in the range of $\lesssim 1$ day to $\gtrsim 100$ days. Earlier attempts to compare the T_B with black hole mass (M_{BH}) for AGNs have shown a rough linear scaling but with a scatter (Markowitz et al. 2003; McHardy et al. 2004). Improving on it, an inverse dependence on a second variable, probably the accretion rate, was suggested (McHardy et al. 2004, 2005; Uttley & McHardy 2005). McHardy et al. (2006) quantified the relationship between T_B, M_{BH}, and L_{bol} (in place of the accretion rate) as $\log T_B = A \log M_{BH} - B \log L_{bol} + C$, where M_{BH} is in units of 10^6 solar masses and L_{bol} is bolometric luminosity in 10^{44} erg s^{-1}. Best-fit values determined by them are $A = 2.1$, $B = 0.98$, and $C = 2.32$. Using this relation, we have calculated break timescales (T_B) for our AGN sample. Values of $\log(M_{BH})$ (in units of 10^6 $M_\odot$) and $\log(L_{bol})$ (in units of 10^{44} erg s^{-1}) listed in Table 1 are adopted from Woo & Urry (2002), Uttley & McHardy (2005), and Wandel & Mushotzky (1986). The masses are estimated either using reverberation mapping or the BLR size–luminosity relation or the stellar velocity dispersion method. L_{bol} values are also taken from the references mentioned above. It should be noted that L_{bol} for the blazars may be beamed, leading to wrong estimates of T_B.

Figure 14 shows the ASM variability strength on the scale of 20 days as a function of $\log(T_B)$. Figure 15 shows the BAT variability strength as a function of $\log(T_B)$. Out of 44 AGNs from the BAT sample of Beckmann et al. (2007), black hole masses and bolometric luminosity are available for 20 sources (Uttley & McHardy 2005), and hence T_B could be estimated for these sources. Out of these, 19 sources are common between the ASM and BAT databases. The remaining source is Mrk 3, which is not in the ASM source list. The figure shows some increase in variability of BAT data for the AGN in the neighborhood of 20 days and decreases on both the lower and higher sides. The average variability for $\log(T_B)$ between -1 and $+1.6$ is 62.9 and 53.6 for the ASM and BAT data, respectively, and these values are 27.4 and 16.7 outside this range. The decrease for higher T_B is as expected. The lower variability at lower T_B could be due to a variety of reasons like (1) inclusion of blazars for which the McHardy et al. (2006) relation may not be valid, and (2) at a very low value of T_B, we are sampling the sources at very low frequencies where a second turnover of PSD is likely if the sources are in a state like the low-hard states of Galactic black hole sources.

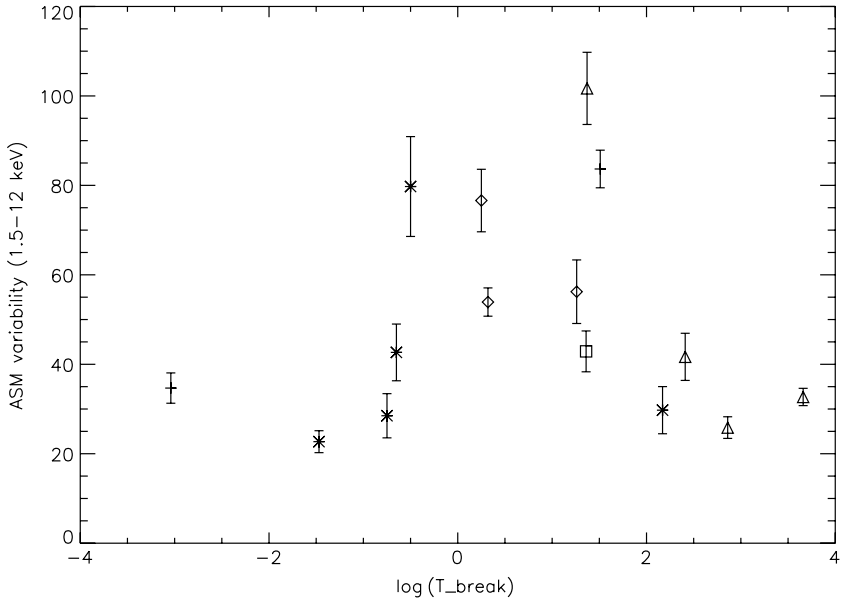

Figure 14. ASM variability strength vs. break timescale (T_B).

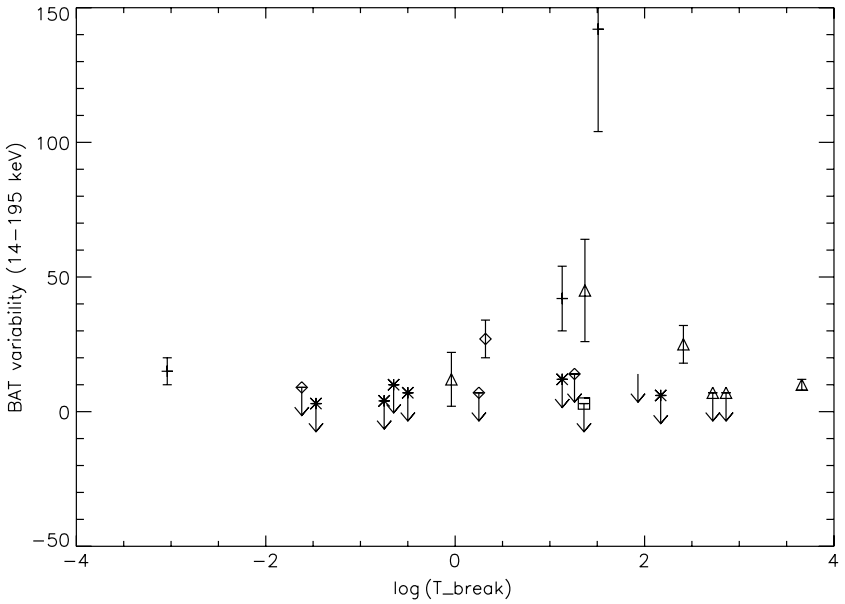

Figure 15. BAT variability strength vs. break timescale (T_B).

3.5. Energy Spectra

We checked for data from pointed observations of these AGNs by X-Ray Telescope (XRT) onboard *Swift* during this nine month period. Data were available for four sources from our list. These were three blazars (3C273, 3C454.3, and Mrk 421) and one Seyfert 2 Galaxy (Cen A). We have fitted spectra over the energy range of 0.3–10 keV for these four objects. For each of these objects, source and background photons were selected using XSELECT version 2.4. For photon counting (PC) mode source photons were selected in a circular region with radius 20 pixels (i.e., 47 arcseconds), whereas background photons were extracted from a nearby circular region with a radius of 40 pixels. For data collected in Windowed Timing (WT) mode, source photons were extracted using the box region with length of 40 pixels and width about 20 pixels. Events with grades 0–12 and 0–2 were selected for PC and WT mode data, respectively. The spectral data were rebinned by GRPPHA 3.0.0 with 20 photons per bin. Standard auxiliary response files and response matrices were used.

Spectra for these sources were fitted using XSPEC version 12.3.1 with a model consisting of an absorbed power law over the energy range of 0.3–10 keV. In each case, N_H was fixed to the value given in Table 2 of Beckmann et al. (2007). Power-law indices and 2–10 keV flux obtained from the fit are given in Table 3. It should be noted here, however, that the *Swift* observations may not be equal to the average photon index representing the ASM observations.

Among the three blazars, Mrk 421 has the steepest spectrum and 3C 454.3 has the flattest one. In the case of 3C454.3, we have not estimated the variability strength in the ASM band because of the low count rate. ASM variability strengths for

the other two blazars are 83.7 ± 4.2 for Mrk 421 and 34.7 ± 3.4 for 3C273. The BAT variability strengths of these three sources arranged in order of increasing power-law index are: 3C454.4 (42 ± 12), 3C273 (15 ± 5) and Mrk 421 (142 ± 38). This indicates an increase in variability strength for sources with steeper spectra. But this inference should be taken with caution. It should be noted that in the case of Mrk 421, which is a BL Lac-type object, the hard X-ray band is dominated by high-energy synchrotron emission, whereas in the case of 3C454.3 and 3C273, which are FSRQ, hard X-ray emission is mainly inverse-Compton emission. This could be one possible reason for the steeper spectrum of Mrk 421 compared to the other two objects. It is also quite possible that the long-duration variabilities of blazars are influenced by infrequent strong flare events and the higher variability in any one blazar could simply be the effect of a few large events which happen to occur in that source.

4. DISCUSSION AND CONCLUSIONS

The study of X-ray variability of AGNs at longer timescales and also at different energies is very important to pin down the accretion disk geometry and the radiation processes involved in X-ray emission very close to black holes. We have made a systematic study of the soft X-ray variability characteristics of all AGNs with measured long timescale variability from *Swift*/BAT.

One of the important findings of this work is that individual ASM dwells can be co-added to obtain flux integrated over long timescales and by propagating the measurement errors, very low errors on the data points are obtained. This method assumes that most of the systematic errors in the flux measurements in the individual dwell measurements are understood and taken care of. Support for this assumption comes from the fact that the long-duration light curves of several AGNs bear a striking similarity to the light curves obtained from pointed *RXTE*/PCA observations. Some more work, however, need to be done to understand possible time-dependent systematic errors so that a complete data set can be used to derive meaningful power spectral densities.

Another important finding is the quite uniform variation of variability strength with energy for diverse classes of objects, except for the blazar Mrk 421. For this particular source, there is a marked increase in the variability as a function of energy. Such behavior has been observed at shorter durations. Horan et al. (2009) made a detailed multiwavelength study for a period of about 300 days and find the variability to increase across the full electromagnetic band (see previous work by Giebels et al. 2007). In particular, they noticed a sharp increase of variability from soft X-rays to hard X-rays: the values for variability ($F_{\rm var}$) were 26.9, 44.3, 52.9, and 99.3, respectively, for *Swift*/XRT, *RXTE*/ASM, *RXTE*/PCA, and *Swift*/BAT data (for observation bins of a few tens of thousand seconds and duration in the range of 24–256 days). The values that we obtained are 79 (*RXTE*/ASM 1.5–3 keV), 88 (*RXTE*/ASM 3–12 keV) for 12.5 years, and 142 (*Swift*/BAT for 300 days). The energy-dependent variability behavior of the blazar in our list, 3C 273, for which data are available in both the soft and hard X-ray bands, shows an energy-dependent behavior similar to Seyfert 1 galaxies. McHardy (2006) has noted that the wide band PSD of 3C273 is identical to that of Seyfert galaxies and contended that the process responsible for variability in this source is the same one that produces variability in nonbeamed sources.

Most of the other sources in our sample are Seyfert galaxies, and a decrease in the variability as a function of energy is observed. In a detailed study of a large number of Seyfert galaxies based on the first seven years of *RXTE*/PCA monitoring, Markowitz & Edelson (2004) give energy-dependent variability data for long durations and a similar trend of decrease in variability with energy has been noticed. There are five Seyfert 1 galaxies (3C120, 3C390.3, IC4329A, NGC3783, and MCG-6-30-15) and two Seyfert 1.5 galaxies (NGC4151 and NGC3227) common between their sample and our work. The ratios of variability for the soft (2–4 keV) and the hard (7–12 keV) bands are, respectively, 1.15, 1.26, 1.19, 1.28, 1.37, 1.26, and 1.35, for a duration of 216 days. For comparison, similar ratios from our data (1.5–3 keV versus 3–12 keV) for the above sources are, respectively, are 1.65, 1.62, 2.65, 2.9, 1.71, 2.6, and 2.5 for the full ASM duration. The typical uncertainties are 0.06 for the *RXTE* data and 0.3 for our data. Though this ratio from *RXTE* data is fairly similar for all the sources (about 1.27), for the ASM data it varies from 1.66 to 2.64. For five sources, energy-dependent variability at longer timescales (> 16 days) is given by Markowitz et al. (2003) and for two of the sources, where we have obtained very high ratios (NGC 3783 and NGC 4151), a sharp upturn toward lower energies is noticed (see their Figure 6). Further, *RXTE*/ASM is more sensitive to low-energy X-rays. The effective area at 2 keV is about 33% of the effective area at 5 keV (Levine et al. 1996), whereas this number is < 1% for *RXTE*/PCA (Jahoda et al. 2006), mainly due to the propane layer on the top side of *RXTE*/PCA which has lower transparency at low energies due to aluminized mylar windows and the permeation of xenon gas into the propane layer (Jahoda et al. 1996). Hence it is quite possible that the higher variability at low energies derived by us is real and indicates a sharp increase of variability in AGNs at lower energies for longer timescales. Though we cannot completely rule out some further systematic errors, it is quite evident that *RXTE*/ASM is a unique instrument to probe long timescale variability at lower energies.

There are, indeed, several indicators from early *EXOSAT* data which support the above assertion. Walter & Courvoisier (1992) discuss X-ray variability of several AGNs observed by *EXOSAT* over the period of a year and note that soft X-rays vary by factors up to 7, much higher than that seen in hard X-rays. Two of the sources in their list are common to the present work: MR2251-178 and NGC 3783. For these two sources, they report a peak-to-peak variation of 4.5 and 3, respectively, in the soft X-rays, compared to 1.9 and 1.8 in hard X-rays. This should be compared with the $S_{\rm V}$ derived by us for these two sources: 97 and 67, respectively, in the 1.5–3 keV band and 42 ± 14 and 24 ± 7 in the 3–12 keV band, respectively. Though there is a strong indication of very high soft X-ray variability at long timescales, a detailed comparison with a large number of pointed observations for individual sources is required to pin down any residual systematic errors in the *RXTE*/ASM data.

Energy-dependent variability has been studied extensively in Galactic black hole sources (see Zdziarski 2005 and references therein) and one of the models used to explain the energy dependency is the variations in the input parameters of the thermal Comptonization process which results in an pivoting power-law spectrum. Though the very low value of variability in the BAT energy band may be influenced by a nonvarying spectral component in this energy band (like reflection), detailed wideband spectroscopy of Seyfert galaxies suggests a common continuous phenomena for the decreasing variability with increasing

energy. For example, the radio galaxy 3C120 shows only a moderate reflection component and very strong spectral variability (over two days) with the spectral index correlated with the soft X-ray flux, indicating a phenomenon where the input seed photon variation for a thermal Comptonization process causes the energy-dependent X-ray variability (Zdziarski & Grandi 2001). If the same phenomenon is responsible for most of the sources reported in this work, it suggests that (1) for a majority of AGNs the thermal Comptonization is the dominant process, and (2) the pivot energy is higher (greater than about 20 keV).

This work is based on the results provided by the ASM/*RXTE* teams at MIT and at the *RXTE* SOF and GOF at NASA's Goddard Space Flight Center (see previous work by Giebels et al. 2007). This research has also made use of data obtained from the High Energy Astrophysics Science Archive Research Center (HEASARC) provided by NASA's Goddard Space Flight Center. We are very grateful to the referee of this paper for very thoughtful and critical comments.

REFERENCES

Almaini, O., et al. 2000, MNRAS, 315, 325
Arévalo, P., McHardy, I. M., Markowitz, A., Papadakis, I. E., Turner, T. J., Miller, L., & Reeves, J. 2008, MNRAS, 387, 279
Barr, P., & Mushotzky, R. F. 1986, Nature, 320, 421
Beckmann, V., et al. 2007, A&A, 475, 827
Done, C., & Gierlinski, M. 2005, MNRAS, 364, 208
Edelson, R., & Nandra, K. 1999, ApJ, 514, 96
Emmanoulopoulos, D., & Wagner, S. J. 2007, in ASP Conf. Ser. 373, The Central Engine of Active Galactic Nuclei, ed. L. C. Ho & J.-M. Wang (San Francisco, CA: ASP), 163
Giebels, B., Dubus, G., & Khelifi, B. 2007, A&A, 462, 29
Gilfanov, M., & Arefiev, V. 2005, arXiv:astro-ph/0501215
Gliozzi, M., Sambruna, R. M., Jung, I., Krawczynski, H., Horan, D., & Tavecchio, F. 2006, ApJ, 646, 61
Grimm, H.-J., Gilfanov, M., & Sunyaev, R. 2002, A&A, 391, 923
Grupe, D., Thomas, H. C., & Beuermann, K. 2001, A&A, 367, 470
Horan, D., et al. 2009, ApJ, 695, 596
Jahoda, K., et al. 1996, Proc. SPIE, 2808, 59
Jahoda, K., et al. 2006, ApJS, 163, 401
Levine, A. M., et al. 1996, ApJ, 469, L33
Markowitz, A., & Edelson, R. 2001, ApJ, 547, 684
Markowitz, A., & Edelson, R. 2004, ApJ, 617, 939
Markowitz, A., et al. 2003, ApJ, 593, 96
McHardy, I. M. 1988, Mem. Soc. Astron. Ital., 59, 239
McHardy, I. M. 2006, ASPC, 350, 94
McHardy, I. M., & Czerny, B. 1987, Nature, 325, 696
McHardy, I. M., Gunn, K. F., Uttley, P., & Goad, M. R. 2005, MNRAS, 359, 1469
McHardy, I. M., Koerding, E., Knigge, C., Uttley, P., & Fender, R. P. 2006, Nature, 444, 730
McHardy, I. M., Papadakis, I. E., Uttley, P., Page, M. J., & Mason, K. O. 2004, MNRAS, 348, 783
Nandra, K., George, I. M., Mushotzky, R. F., Turner, T. J., & Yaqoob, T. 1997, ApJ, 476, 70
Sanders, J. S., & Fabian, A. C. 2007, MNRAS, 381, 1381
Swank, J. 1999, Nucl. Phys. B, 69, 12
Tueller, J., et al. 2008, ApJ, 681, 113
Uttley, P., & McHardy, I. M. 2004, Prog. Theor. Phys. Suppl., 155, 170
Uttley, P., & McHardy, I. M. 2005, MNRAS, 363, 586
Uttley, P., McHardy, I. M., & Papadakis, I. E. 2002, MNRAS, 332, 231
Vaughan, S., Edelson, R., Warwick, R. S., & Uttley, P. 2003, MNRAS, 345, 1271
Walter, R., & Courvoisier, T. J.-L. 1992, A&A, 266, 57
Wandel, A., & Mushotzky, R. F. 1986, ApJ, 306, L61
Winter, L. M., Mushotzky, R. F., Reynolds, C. S., & Tueller, J. 2009, ApJ, 690, 1322
Woo, J.-H., & Urry, C. M. 2002, ApJ, 579, 530
Zdziarski, A. A. 2005, MNRAS, 360, 816
Zdziarski, A. A., & Grandi, P. 2001, ApJ, 551, 186